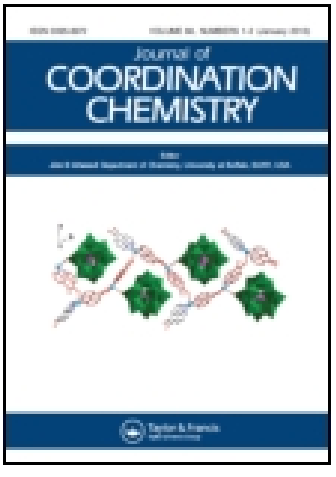

Journal of Coordination Chemistry
Publication details, including instructions for authors and subscription information:
http://www.tandfonline.com/loi/gcoo20

Two coordination polymers with 3-hydrazino-4-amino-1,2,4-triazole as ligand: synthesis, crystal structures, and non-isothermal kinetic analysis

Cai-Xia Xu[a], Xin Yin[a], Xin Jin[a], Piao He[a], Jian Qin[a], Jian-Guo Zhang[a] & Jian-She Jiao[b]

[a] State Key Laboratory of Explosion Science and Technology, Beijing Institute of Technology, Beijing, China

[b] General Armament Department, Research Institute of FA and ADA Equipment and Technology, Beijing, China

Accepted author version posted online: 18 Jun 2014.Published online: 17 Jul 2014.

To cite this article: Cai-Xia Xu, Xin Yin, Xin Jin, Piao He, Jian Qin, Jian-Guo Zhang & Jian-She Jiao (2014) Two coordination polymers with 3-hydrazino-4-amino-1,2,4-triazole as ligand: synthesis, crystal structures, and non-isothermal kinetic analysis, Journal of Coordination Chemistry, 67:11, 2004-2015, DOI: 10.1080/00958972.2014.936405

To link to this article: http://dx.doi.org/10.1080/00958972.2014.936405

Journal of Coordination Chemistry, 2014
Vol. 67, No. 11, 2004–2015, http://dx.doi.org/10.1080/00958972.2014.936405

Two coordination polymers with 3-hydrazino-4-amino-1,2,4-triazole as ligand: synthesis, crystal structures, and non-isothermal kinetic analysis

CAI-XIA XU†, XIN YIN†, XIN JIN†, PIAO HE†, JIAN QIN†, JIAN-GUO ZHANG*† and JIAN-SHE JIAO‡

†State Key Laboratory of Explosion Science and Technology, Beijing Institute of Technology, Beijing, China
‡General Armament Department, Research Institute of FA and ADA Equipment and Technology, Beijing, China

(*Received 26 March 2014; accepted 4 May 2014*)

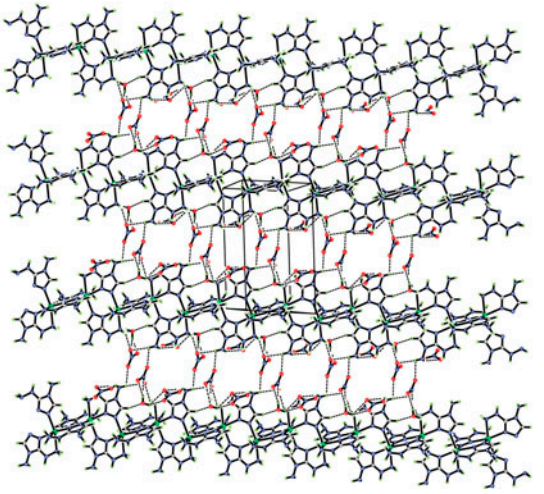

Two coordination polymers, $[Mn_2(HATr)_4(NO_3)_4{\cdot}2H_2O]_n$ (**1**) and $[Cd_2(HATr)_4(NO_3)_4{\cdot}H_2O]_n$ (**2**), were obtained from the corresponding metal nitrate with 3-hydrazino-4-amino-1,2,4-triazole (HATr) and characterized through elemental analysis and IR spectroscopy. The structures were determined by single-crystal X-ray diffraction. The results show that both complexes crystallize in the triclinic *P-1* space group and have six-coordinate distorted octahedral structures, which are made up of infinite 1-D chains running along the *a* axis of metals linked by bridging-chelating HATr ligands. The coordination sites are in agreement with the computational results. Additionally, the decomposition temperatures were determined by differential scanning calorimetry and the kinetic parameters were calculated using Kissinger's and Ozawa–Doyle's methods; the energies of combustion for **1** and **2** were −7186.25 and −6922.53 kJ M^{-1} and the enthalpies of formation were obtained as −1002.35 and −457.27 kJ M^{-1}, respectively.

*Corresponding author. Email: zjgbit@bit.edu.cn

Keywords: Coordination polymers; 3-Hydrazino-4-amino-1,2,4-triazole; Crystal structure; Thermal analysis

1. Introduction

In pursuit of high nitrogen energetic materials, metal complexes with nitrogen-rich heterocycles [1–5], hydrazine [6], guanidine [7], and other N donor ligands [8, 9] have attracted attention. As polydentate building blocks, 1,2,4-triazole and its derivatives combine the coordination geometries of both pyrazoles and imidazoles, exhibiting a strong ability to bridge metal ions to afford polynuclear structures [10]. More practically, substituted 1,2,4-triazoles are excellent ligands of energetic complexes, such as 4-amino-1,2,4-triazole [11–13], 3,5-diamino-1,2,4-triazole [14], and 3-azido-1,2,4-triazole [15]. Recently, MOFs [16] as a new concept for coordination polymers have attracted interest since the structure and the stability can be improved. Pang and co-workers [17] reported that 3-D energetic MOFs based on 4,4′-azo-1,2,4-triazole resolve the conflict of insensitivity and high energy, which are important for the next generation of explosives.

3-Hydrazino-4-amino-1,2,4-triazole (HATr) with nitrogen content of 73.65% is of interest as an energetic ligand to transitional metal complexes by Ilyushin and co-authors in 1993 [18]. They reported that HATr is a N,N-bidentate ligand, in which N1 and N2 of the triazole are coordinated. In 2003, Ugryumov *et al.* [19] used the same ligand to prepare cobalt(II), copper(II), nickel(II), and cadmium(II) perchlorate complexes, in which the copper complex shows the most effective light-sensitive properties as a laser-ignition explosive. Ilyushin *et al.* [20] further studied the influence of various additives on the threshold of laser initiation of the copper perchlorate complex with HATr as a ligand in 2012. However, there are only these reports available concerning HATr, and there is a lack of information about the crystal structures of the metal complexes containing HATr.

Bearing this in mind, we prepared two HATr complexes, $[Mn_2(HATr)_4(NO_3)_4{\cdot}2H_2O]_n$ (**1**) and $[Cd_2(HATr)_4(NO_3)_4{\cdot}H_2O]_n$ (**2**), which report the crystal structures for the first time, and studied non-isothermal kinetic analysis, energies of combustion as well as enthalpies of formation.

2. Experimental

2.1. *Materials and methods*

All chemical reagents and solvents of analytical grade were obtained from commercial sources and used without purification unless stated otherwise. HATr·2HCl was prepared referring to the literature [21], starting from the reaction of the triaminoguanidinium monohydrochloride with formic acid and hydrochloric acid as catalytic agent under reflux. The yield was 94%.

Elemental analyses were performed on a flash EA 1112 full automatic trace element analyzer. The Fourier transform infrared (FT-IR) spectra were recorded on a Nexus-470 FT-IR (Nicolet) spectrometer (KBr pellet) from 4000 to 400 cm^{-1} with resolution of 6 cm^{-1}. Differential scanning calorimetry (DSC) was carried out on a model Pyris-1 differential scanning calorimeter in static air. A sample of about 0.2 mg was sealed in aluminum pans

for DSC with various heating rates [(5, 10, 15, and 20) °C min^{-1}]. The non-isothermal kinetic parameters were computed by the Kissinger [22] and Ozawa–Doyle [23] equations using the different peak temperatures, obtained in the thermal decomposition process with various heating rates. The combustion heats of **1** and **2** were measured by oxygen bomb calorimetry (Parr 6200, USA) with samples of 0.5 g.

2.2. *Synthesis of HATr*

Sodium hydrogen carbonate (3.36 g, 0.04 M) was slowly added to a solution of HATr·2HCl (3.74 g, 0.02 M) in 10 mL of distilled water. The mixture was stirred until there was no gas released and then the water was evaporated under vacuum, the mixture was dissolved in 30 mL absolute methanol and the inorganic salt was removed by filtration. After filtering, the solvent was removed under reduced pressure to produce a light pink solid at 78% yield. ($C_2H_6N_6$) Anal. Calcd (%): C, 21.05; H, 5.30; N, 73.65. Found: C, 21.15; H, 5.43; N, 73.42. IR (KBr, cm^{-1}): 3399, 3291, 3152, 1650, 1630, 1584, 1552, 1006.

2.3. *Synthesis of 1 and 2*

A solution of $Mn(NO_3)_2$ (50 wt%, 1.79 g) or $Cd(NO_3)_2·4H_2O$ (1.54 g, 0.005 M) in 15 mL absolute methanol was added dropwise to the solution of HATr (1.14 g, 0.01 M) in 30 mL absolute methanol under stirring. After 1 h, the precipitate was collected by filtration, rinsed with distilled water, and dried in air. The yields were 36.4% for **1** and 38.2% for **2**.

Anal. Calcd for **1** (%): C, 11.30; H, 3.32; N, 46.12. Found: C, 11.35; H, 3.34; N, 46.32. IR (KBr, cm^{-1}): 3434, 3284, 3243, 3151, 1679, 1655, 1577, 1384, 1036, 822.

Anal. Calcd for **2** (%): C, 10.14; H, 2.77; N, 41.40. Found: C, 10.07; H, 2.75; N, 40.82. IR (KBr, cm^{-1}): 3320, 3273, 3153, 1675, 1655, 1578, 1384, 1037, 823.

2.4. *X-ray single-crystal determination*

A Rigaku AFC-10/Saturn 724+ CCD diffractometer with graphite monochromated MoK_α radiation ($\lambda = 0.071073$ nm) was applied for structure analyses. The data were collected at 143 K for **1** and 153 K for **2** using φ and ω scan modes. The structure was solved by direct methods using SHELXS-97 [24, 25] and refined by full-matrix least-squares procedures on F^2 with SHELXL-97 [26]. The CIF files were checked at the checkCIF website. All non-hydrogen atoms were obtained from the difference Fourier map and refined anisotropically. All hydrogens were generated geometrically, assigned appropriated isotropic thermal parameters, and included in structure factor calculations. Crystallographic data and experimental details for structure analyses are summarized in table 1.

3. Results and discussion

3.1. *Theoretical computation*

All electronic structure calculations were carried out using the Gaussian03 program package [27]. The geometric optimization of HATr was carried out using B3-LYP functional with

Table 1. Crystal data and structure refinement details for **1** and **2**.

Complex	**1**	**2**
Empirical formula	$C_8H_{28}Mn_2N_{28}O_{14}$	$C_8H_{26}Cd_2N_{28}O_{13}$
Formula mass	850.46	947.37
Temperature (K)	143(2)	153(2)
Crystal dimensions (mm)	0.43 × 0.39 × 0.36	0.36 × 0.06 × 0.05
Crystal system	Triclinic	Triclinic
Space group	*P-1*	*P-1*
Z	2	2
a, b, c (Å)	8.076(2), 12.670(3), 15.131(4)	8.149(2), 12.850(4), 15.218(4)
α, β, γ (°)	91.020(3), 94.709(4), 100.646(5)	91.946(4), 94.533(5), 101.076(6)
Cell volume (Å^3)	1515.7(6)	1557.0(8)
D_{Calcd} (g cm^{-3})	1.864	2.021
μ (MoK$_\alpha$) (mm^{-1})	0.71073	0.71073
F (0 0 0)	868	940
θ (°)	2.58–25.04	2.56–30.50
h, *k*, and *l* range	−9 to 9, −15 to 15, −18 to 18	−10 to 11, −18 to 18, −21 to 21
Reflections collected	12,539	20,918
Reflections unique [R_{int}]	5316 [R_{int} = 0.0234]	9322 [R_{int} = 0.0359]
Data/restraint/parameter	5316/0/595	9322/6/473
Goodness-of-fit on F^2	1.058	1.003
R_1, wR_2 [$I > 2\sigma(I)$]	R_1 = 0.0361, wR_2 = 0.0879[a]	R_1 = 0.0596, wR_2 = 0.1459[b]
R_1, wR_2 (all data)	R_1 = 0.0411, wR_2 = 0.0916[a]	R_1 = 0.0858, wR_2 = 0.1626[b]
$\Delta\rho_{max}$, $\Delta\rho_{min}$ (e Å^{-3})	0.563, −0.346	4.237, −1.619

[a] $w = 1/[\sigma^2(F_o^2) + (0.0448p)^2 + 1.0228p]$, where $p = (F_o^2 + 2F_c^2)/3$.
[b] $w = 1/[\sigma^2(F_o^2) + (0.0698p)^2 + 9.9600p]$, where $p = (F_o^2 + 2F_c^2)/3$.

6-311 + G** basis set [28]. The optimized structure was characterized to be true local energy minima on the potential energy surface without imaginary frequencies.

Natural bond orbital analysis is a simple and reasonable tool to study the possible coordination sites and in frontier molecular orbitals, the highest occupied molecular orbital (HOMO) represents the ability to donate an electron, the lowest unoccupied molecular orbital (LUMO) as an electron acceptor represents the ability to obtain an electron [29]. The atomic NBO charges of HATr molecule (figure 1) are listed in table 2, and figure 2 shows the HOMO and LUMO of HATr group. In HATr, all nitrogens have negative charges. However, it is obvious that N4 and N6 atoms are conjugated with the π-system of triazole ring,

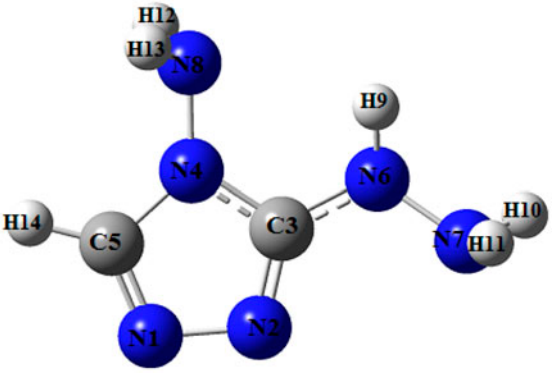

Figure 1. Molecular unit and the atomic numbering scheme of HATr.

Table 2. Selected NBO charges of HATr at the B3LYP/6-311 + G** level.

Atom	Charge	Atom	Charge	Atom	Charge
N1	−0.29	N4	−0.30	N6	−0.47
N2	−0.36	N8	−0.64	N7	−0.62

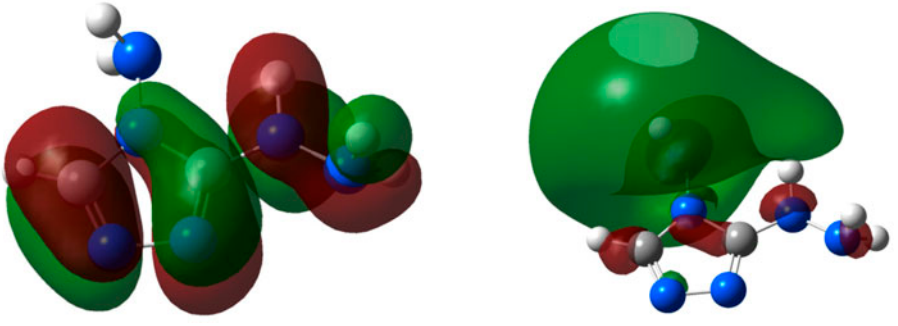

Figure 2. HOMO (left) and LUMO (right) of HATr.

so it is impossible for N4 and N6 to coordinate. Furthermore, the HOMO shows that the electrons are located mainly in the triazole ring and hydrazine group. Finally, N1, N2, and N7 are the possible coordination sites, which is testified by the experimental results in the crystal structure of **1** and **2**.

3.2. *Structure description*

The X-ray structural analysis indicates that **1** and **2** are isostructural, belonging to the triclinic system with space group *P-1*. The least asymmetric molecular unit consists of two metal cations, four neutral HATr ligands, four NO_3^- anions, two crystal waters, and a water of crystallization for **1** and **2**. Selected bond lengths and angles for **1** and **2** are listed in tables 3 and 4.

Each central metal is coordinated octahedrally by two 2-site nitrogens of the triazole ring and two terminal nitrogens of hydrazine from two HATrs, and two 1-site nitrogens from another two HATrs (figure 3). The bond lengths of Mn–N are between 2.204(18) and 2.329 (2) Å with an average of 2.252 Å in **1**, whereas in **2**, the Cd–N bond lengths are between 2.299(4) and 2.422(5) Å with an average of 2.349 Å. The octahedral coordination sphere is Jahn–Teller distorted along the N6–M–N1A axis (e.g. Mn1–N6 = 2.314(2) Å, Mn1–N1A = 2.216(2) Å; Cd1–N6 = 2.414(4) Å, and Cd1–N1A = 2.312(4) Å). The N–M–N angles (e.g. <(N7B–Mn1–N8) = 95.38(7)°, <(N8–Mn1–N12) = 72.75(7)°, <(N7B–Cd1–N8) = 93.51 (14)°, and <(N8–Cd1–N12) = 70.71(15)°) in the N7B–N8–N12–N2 plane deviate from 90° and indicate a distorted octahedral coordination sphere which is induced by the fixed geometry of the HATr ligand.

In each metal complex, HATr is a chelating and bridging ligand with three coordination sites at the same time. For **1** as an example, two five-member planar chelate rings were formed by one Mn ion and two HATrs, resulting in minimum steric hindrance. Plane

Table 3. Selected bond lengths (Å) and angles (°) for **1**.

Mn1–N2	2.204(18)	N1–N2	1.402(3)
Mn1–N1A$^{\#1}$	2.216(2)	N2–C2	1.318(3)
Mn1–N6	2.314(2)	N3–C1	1.360(3)
Mn1–N8	2.223(19)	N3–C2	1.345(3)
Mn1–N12	2.329(2)	N3–N4	1.406(2)
Mn1–N7B$^{\#2}$	2.227(19)	N5–C2	1.342(3)
N1–C1	1.302(3)	N5–N6	1.425(3)
N2–Mn1–N1A$^{\#1}$	93.05(7)	C2–N2–Mn1	112.67(15)
N2–Mn1–N7B$^{\#2}$	101.84(7)	N1–N2–Mn1	140.77(14)
N1A$^{\#1}$–Mn1–N7B$^{\#2}$	91.54(7)	C1–N1–N2	107.10(19)
N2–Mn1–N8	160.33(7)	C1–N1–Mn1A$^{\#1}$	126.42 (16)
N1–Mn1–N8	95.95(7)	N2–N1–Mn1A$^{\#1}$	126.09(14)
N8–Mn1–N7B$^{\#2}$	95.38(7)	C2–N3–C1	105.93(19)
N1–Mn1–N6	167.21(7)	C1–N3–N4	130.90(2)
N2–Mn1–N6	74.19(7)	C2–N3–N4	122.90(2)
N7B$^{\#2}$–Mn1–N6	90.27(8)	C2–N5–N6	114.00(18)
N8–Mn1–N6	96.48(7)	N5–N6–Mn1	109.98(14)
N1–Mn1–N12	92.08(9)	N1–C1–N3	110.2(2)
N2–Mn1–N12	89.51(7)	N2–C2–N5	126.0(2)
N7A$^{\#1}$–Mn1–N12	167.89(8)	N2–C2–N3	110.2(2)
N6–Mn1–N12	88.76(9)	N5–C2–N3	123.7(2)
N8–Mn1–N12	72.75(7)	C2–N2–N1	106.53(18)

Note: Symmetry transformations used to generate equivalent atoms: #1 $-x+1$, $-y+1$, $-z+2$, #2 $-x$, $-y+1$, $-z+2$.

Table 4. Selected bond lengths (Å) and angles (°) for **2**.

Cd1–N2	2.299(4)	N1–N2	1.404(6)
Cd1–N1A$^{\#1}$	2.312(4)	N2–C2	1.330(6)
Cd1–N6	2.414(4)	N3–C2	1.355(6)
Cd1–N8	2.324(4)	N3–C1	1.361(7)
Cd1–N12	2.422(5)	N3–N4	1.402(6)
Cd1–N7B$^{\#2}$	2.323(4)	N5–C2	1.339(7)
N1–C1	1.306(7)	N5–N6	1.436(6)
N2–Cd1–N1A$^{\#1}$	95.06(15)	C1–N1–Cd1A$^{\#1}$	125.8(4)
N2–Cd1–N7B$^{\#2}$	95.92(15)	N2–N1–Cd1A$^{\#1}$	125.0(3)
N1A$^{\#1}$–Cd1–N7B$^{\#2}$	90.46(16)	C2–N2–N1	106.6(4)
N2–Cd1–N8	168.40(15)	C2–N2–Cd1	112.9(3)
N1A$^{\#1}$–Cd1–N8	91.60(15)	N1–N2–Cd1	139.8(3)
N7B$^{\#2}$–Cd1–N8	93.51(14)	C2–N3–C1	106.1(4)
N2–Cd1–N6	71.90(15)	C2–N3–N4	122.4(5)
N1A$^{\#1}$–Cd1–N6	165.91(15)	C1–N3–N4	130.8(5)
N7B$^{\#2}$–Cd1–N6	96.07(16)	C2–N5–N6	115.5(4)
N8–Cd1–N6	100.41(15)	N5–N6–Cd1	109.4(3)
N2–Cd1–N12	99.44(15)	N1–C1–N3	110.3(5)
N1A$^{\#1}$–Cd1–N12	92.77(17)	N2–C2–N5	126.3(5)
N7B$^{\#2}$–Cd1–N12	163.96(16)	N2–C2–N3	109.7(4)
N6–Cd1–N12	84.38(17)	N5–C2–N3	123.9(5)
N8–Cd1–N12	70.71(15)	C1–N1–N2	107.3(4)

Note: Symmetry transformations used to generate equivalent atoms: #1 $-x+1$, $-y+1$, $-z$, #2 $-x+2$, $-y+1$, $-z$.

equations are: A, $-1.742x - 2.261y + 14.711z = 12.7432$ (mean deviation, 0.0756 Å) for [Mn1, N2, C2, N5, N6] and B, $2.444x + 11.101y + 0.570z = 6.1676$ (mean deviation, 0.0926 Å) for [Mn1, N8, C4, N11, N12], respectively, The angle between planes A and B is 100.7°. One six-member planar ring was formed by four 1-site and 2-site nitrogens of triazole ring bridging two Mn ions, and the equation is: C, $-2.091x - 1.332y + 14.768z = 13.0565$ (mean

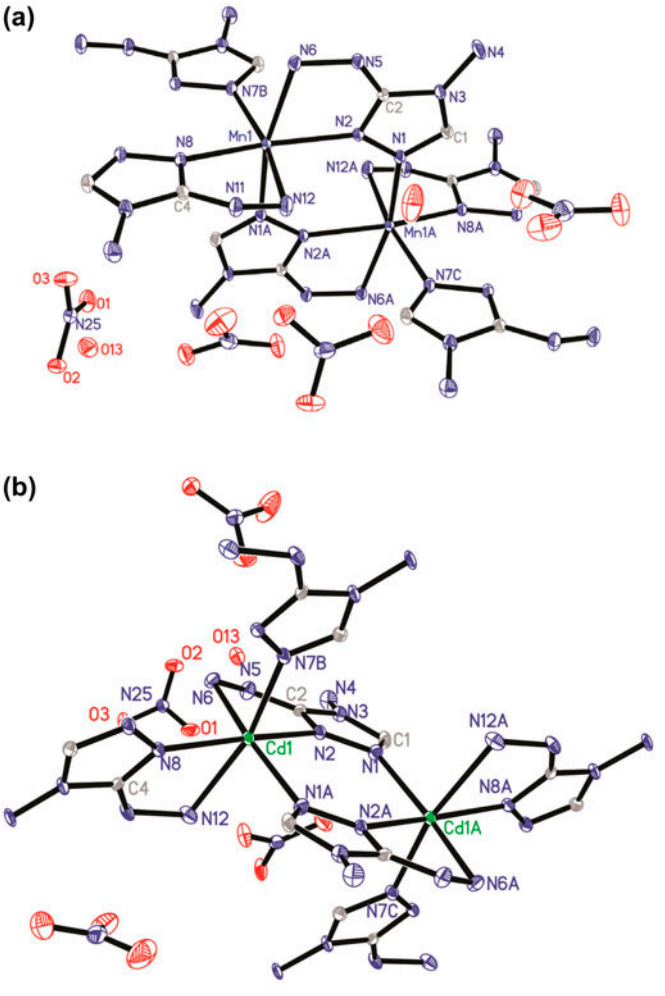

Figure 3. Coordination environment of the Mn^{2+} in **1** (a) and Cd^{2+} in **2** (b). All hydrogens are omitted for clarity; thermal ellipsoids are drawn at the 30% probability level.

deviation, 0.0140 Å) for [Mn1, N2, N1, Mn1A, N2A, N1A], the angle between the planes A and C is 4.5° and B and C is 97.8°.

The five-member and six-member rings give linear chains along the *a* axis, thus, a 1-D coordination polymer is formed. Moreover, these 1-D polymeric chains are further connected via hydrogen bonds forming a 2-D network structure in **2** (figure 4), all oxygens of nitrate are acceptors in hydrogen bonds to nitrogens of amino and hydrazine groups from HATr ligands or oxygens of crystal water.

3.3. *IR spectroscopy*

The compounds were investigated through IR spectroscopy. The assignments of absorptions were undertaken referring to values in the literature [30]. Strong

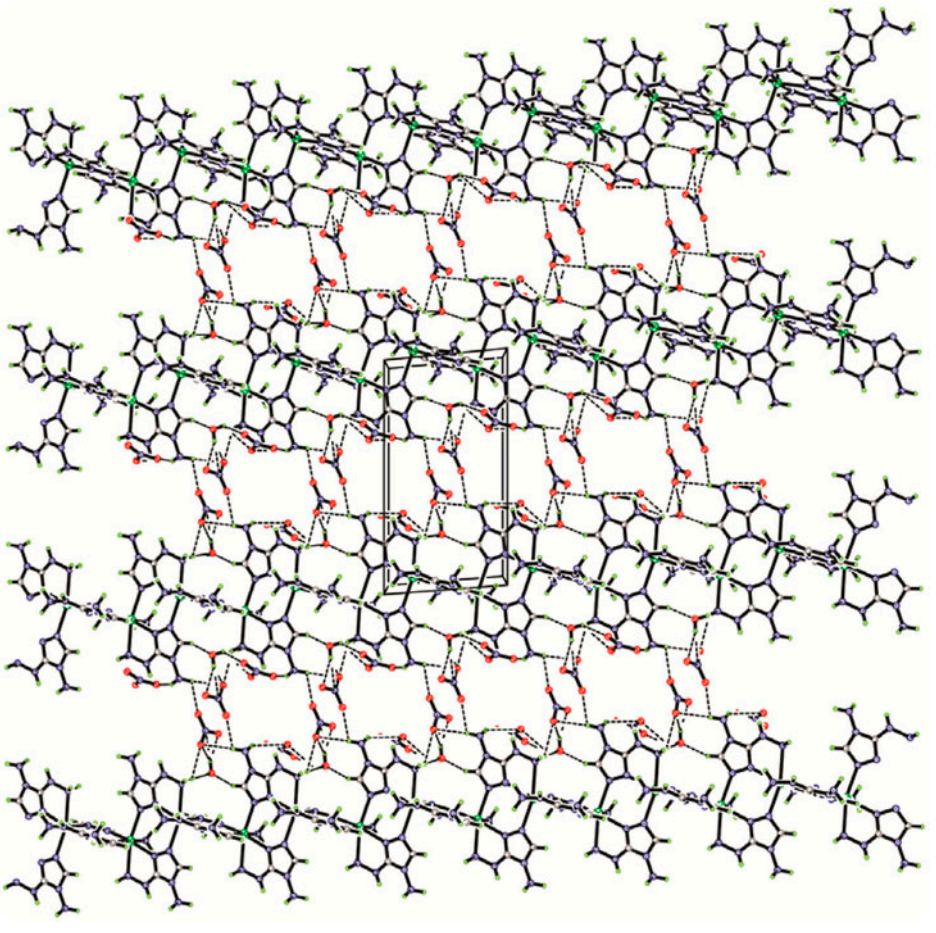

Figure 4. A view of hydrogen bonds (dotted lines) linking the polymeric chains in **2**.

absorptions are observed in spectra above 3000 cm^{-1}, indicating N–H and O–H vibrations. Here, the N–H valence vibration of the hydrazine group of the ligand is visible as a relatively sharp absorption band at 3300–3151 cm^{-1}, while the broadened vibrations around 3400 cm^{-1} can be attributed to the absorptions of hydrogen bonded O–H in complexes.

A relatively strong absorption at 1666–1650 cm^{-1} can be assigned to the C=N vibration of the triazole ring, whereas the N–H valence vibration of NH_2 can be detected by absorptions at slightly lower energy 1630–1577 cm^{-1}. The C=N and N–N vibrations of the triazole ring are shifted upon complexation to higher wave numbers (1655 and 1036 cm^{-1}) for **1** compared with 1650 and 1006 cm^{-1} of free HATr, while the N–H valence vibrations shifted to lower wave number because of strong hydrogen bonds between the amino, hydrazino, and nitrate, for example, from 3291 cm^{-1} in HATr to 3273 cm^{-1} in **2**.

3.4. *Thermal stability and non-isothermal kinetic analysis*

DSC measurements to determine the decomposition temperatures of **1** and **2** were performed at a heating rate of $\beta = 10\ ^\circ\mathrm{C\ min^{-1}}$. Complex **1** decomposed with three exothermic processes, while **2** had two exothermic peaks; the onset decomposition temperatures for **1** and **2** were 260 and 295 °C (figure 5), which showed that both complexes have good thermal stability.

In the present work, Kissinger's and Ozawa–Doyle's methods are used to determine the apparent activation energy (E) and the pre-exponential factor (A). The Kissinger (1) and Ozawa–Doyle (2) equations are as follows:

$$\frac{d\ln(\beta/T_\mathrm{p}^2)}{d(1/T_\mathrm{p})} = -\frac{E_\mathrm{a}}{R} \tag{1}$$

$$\log\beta + \frac{0.4567E_\mathrm{a}}{RT_\mathrm{p}} = C \tag{2}$$

where T_p is the peak temperature, °C; R is the gas constant, $8.314\ \mathrm{J\,M^{-1}\,^\circ C^{1-}}$; β is the linear heating rate, $^\circ\mathrm{C\ min^{-1}}$; and C is a constant.

We can infer that the exothermic process makes a dominant effect on the decomposition of **1** and **2** from the DSC curves. Based on the DSC curves obtained under the conditions of static air at four different heating rates of 5, 10, 15, and $20\ ^\circ\mathrm{C\ min^{-1}}$, the values of the peak temperature T_p (°C), the apparent activation energies E_k and E_o ($\mathrm{kJ\,M^{-1}}$, where subscript k is Kissinger's method and subscript o is Ozawa–Doyle's method), the pre-exponential factor A_k ($\mathrm{S^{1-}}$) and linear coefficients R_k and R_o were determined by Kissinger's method and Ozawa–Doyle's method. The detailed data and calculated kinetic parameters are listed in table 5. The calculated results using both methods correspond well with each other, and they are also all in the normal range of kinetic parameters for the thermal decomposition reaction of solid materials [31]. The Arrhenius equation can be expressed using the

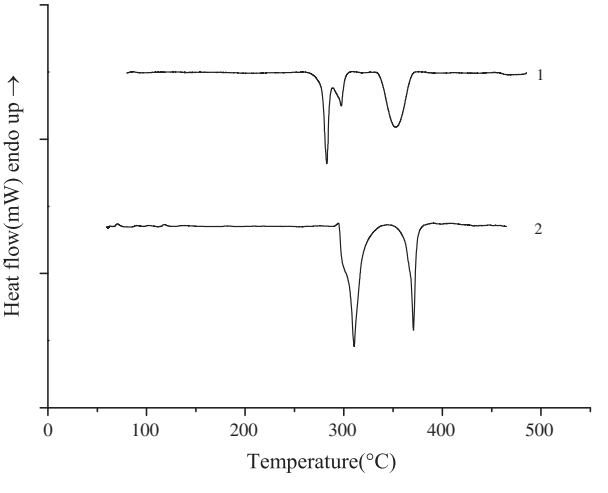

Figure 5. DSC curves of **1** and **2** with a heating rate of $10\ ^\circ\mathrm{C\ min^{-1}}$.

Table 5. Peak temperatures of the first exothermic stage at different heating rates and the kinetic parameters.[a]

	Peak temperatures (°C)	
Heating rates (°C min^{-1})	Complex **1**	Complex **2**
5	269.7	301.0
10	282.9	310.7
15	290.0	314.4
20	294.3	317.7
E_k (kJ M^{-1})/ln(A_k/S^{-1})/R_k	133.4/10.48/–0.9982	223.6/18.16/–0.9949
E_o (kJ M^{-1})/R_o	135.6/–0.9984	221.8/–0.9953

[a]Subscript k: Kissinger's method; Subscript o: Ozawa–Doyle's method; *R*: linear correlation coefficient.

calculators E_a (the average of E_k and E_o) and ln A_k as follows: $\ln k = 10.48–134.5 \times 10^3/RT$ for **1** and $\ln k = 18.16–222.7 \times 10^3/RT$ for **2**. These equations can be used to estimate the rate constants of the initial thermal decomposition process of the complexes.

3.5. *Energies of combustion and enthalpies of formation*

Energy of combustion and formation are significant characteristics to assess the energetic properties of a new compound. In order to study the energies of combustion ($\Delta H = Q_p$) and the enthalpies of formation ($\Delta_f H^\circ_{298}$) of **1** and **2**, constant volume energies of combustion (Q_v) of **1** and **2** were measured by oxygen bomb calorimetry as −7211.9 and −6953.7 kJ M^{-1}, respectively. The bomb combustion reaction equations might be as follows:

$$C_8H_{28}Mn_2N_{28}O_{14} + 10O_2 \longrightarrow 2MnO_2 + 8CO_2 + 14H_2O + 14N_2 \quad (3)$$

$$C_8H_{26}Cd_2N_{28}O_{13} + 9O_2 \longrightarrow 2CdO + 8CO_2 + 13H_2O + 14N_2 \quad (4)$$

and the energies of combustion are as follows:

$$\Delta H(1) = Q_p = Q_v + \Delta nRT = -7186.25\ \text{kJ mol}^{-1} \quad (5)$$

$$\Delta H(2) = Q_p = Q_v + \Delta nRT = -6922.53\ \text{kJ mol}^{-1} \quad (6)$$

So, the energies of combustion for **1** and **2** were −7186.25 and 6922.53 kJ M^{-1}; both were lower than $[Cd(IMI)_2(N_3)_2]_n$ (IMI = imidazole) [32] but higher than $[Mg(CHZ)_3](ClO_4)_2$ (CHZ = carbohydrazide) [6].

These two metal complexes have relatively thermodynamically stable structures. The standard enthalpies of formation of **1** and **2** were back calculated from the energies of combustion on the basis of equations. (3) and (4), and Hess' Law as applied in thermochemical equations (5) and (6). With the known enthalpies of formation of manganese dioxide ($\Delta_f H^\circ_{298}[MnO_2, s] = -519.7$ kJ M^{-1}), cadmium oxide ($\Delta_f H^\circ_{298}[CdO, s] = -258.2$ kJ M^{-1}), carbon dioxide ($\Delta_f H^\circ_{298}[CO_2, g] = -393.5$ kJ M^{-1}), and water ($\Delta_f H^\circ_{298}[H_2O, l] = -285.8$ kJ M^{-1}), the enthalpies of formation of **1** and **2** can now be calculated as:

$$\Delta_f H^\circ_{298}(\mathbf{1}) = 2\Delta_f H^\circ_{298}(MnO_2, s) + 8\Delta_f H^\circ_{298}(CO_2, g) + 14\Delta_f H^\circ_{298}(H_2O, l) - \Delta_c H^\circ(1, s) = -1002.35\,kJ\,mol^{-1} \quad (7)$$

$$\Delta_f H^\circ_{298}(\mathbf{2}) = 2\Delta_f H^\circ_{298}(CdO_2, s) + 8\Delta_f H^\circ_{298}(CO_2, g) + 13\Delta_f H^\circ_{298}(H_2O, l) - \Delta_c H^\circ(2, s) = -457.27\,kJ\,mol^{-1} \quad (8)$$

4. Conclusion

Two new coordination polymers were prepared by reacting HATr with metal nitrates and characterized via elemental analysis and IR spectroscopy. These complexes have a similar configuration. X-ray single-crystal structures of **1** and **2** were obtained for the first time, both central metal ions are six-coordinate with distorted octahedral structures by four nitrogens of two triazole rings and two terminal nitrogens of hydrazine groups. The structures are made up of infinite 1-D chains running along the *a* axis of metal atoms linked by bridging-chelating HATr ligands. Furthermore, polymeric chains are held together forming a 2-D network with hydrogen bounding interactions in **2**. The non-isothermal kinetic analysis results indicate that the Arrhenius equation can be expressed as $\ln k = 10.48–134.5 \times 10^3/RT$ for **1** and $\ln k = 18.16–222.7 \times 10^3/RT$ for **2**, the energies of combustion and enthalpies of formation of **1** and **2** were −7186.25, −6922.53, −1002.35, and −457.27 kJ M^{-1}, respectively.

Supplementary material

Further information concerning the crystal structure determinations in CIF format is available in the Supporting Information from the Cambridge Crystallographic Data Center (CCDC 979485 and 979484; http://www.ccdc.cam.ac.uk/data_request/cif; Cambridge Crystallographic Data Center, 12 Union Road, Cambridge CB2 1EZ, UK; Fax: +44 1223 336033; E-mail: deposit@ccdc.cam.ac.uk).

Funding

We gratefully acknowledge the financial support from the National Natural Science Foundation of China [grant number 10776002] and the project of State Key Laboratory of Science and Technology [grant number ZDKT12-03].

References

[1] M.H. Huynh, M.A. Hiskey, T.J. Meyer, M. Wetzler. *Proc. Nat. Acad. Sci.*, **103**, 5409 (2006).
[2] G.H. Tao, D.A. Parrish, J.M. Shreeve. *Inorg. Chem.*, **51**, 5305 (2012).
[3] X.B. Zhang, Y.H. Ren, W. Li, F.Q. Zhao, J.H. Yi, B.Z. Wang, J.R. Song. *J. Coord. Chem.*, **66**, 2051 (2013).
[4] Z.M. Li, J.G. Zhang, Y. Cui, T.L. Zhang, Y.J. Shu, V.P. Sinditskii, V.V. Serushkin, V.Y. Egorshin. *J. Chem. Eng. Data*, **55**, 3109 (2010).

[5] Z.M. Li, T.L. Zhang, G.T. Zhang, Z.N. Zhou, L. Yang, J.G. Zhang, K.B. Yu. *J. Coord. Chem.*, **66**, 1276 (2013).
[6] Z.M. Li, T.L. Zhang, L. Yang, Z.N. Zhou, J.G. Zhang. *J. Coord. Chem.*, **65**, 143 (2012).
[7] N. Fischer, M. Joas, T.M. Klapötke, J. Stierstorfer. *Inorg. Chem.*, **52**, 13791 (2013).
[8] F. He, K.Z. Xu, H. Zhang, Q.Q. Qiu, J.R. Song, F.Q. Zhao. *J. Coord. Chem.*, **66**, 845 (2013).
[9] Z. Gao, J. Huang, K.-Z. Xu, W.-T. Zhang, J.-R. Song, F.-Q. Zhao. *J. Coord. Chem.*, **66**, 3572 (2013).
[10] J.G. Haasnoot. *Coord. Chem. Rev.*, **200–202**, 131 (2000).
[11] S. Cudziło, M. Nita. *J. Hazard. Mater.*, **177**, 146 (2010).
[12] B.D. Wu, T.L. Zhang, Y. Li, W.C. Tong, Z.N. Zhou, J.G. Zhang, L. Yang. *Z. Anorg. Allg. Chem.*, **639**, 2209 (2013).
[13] S.W. Wang, L. Yang, J.L. Feng, B.D. Wu, J.G. Zhang, T.L. Zhang, Z.N. Zhou. *Z. Anorg. Allg. Chem.*, **637**, 2215 (2011).
[14] Q. Yang, Q. Wei, S.P. Chen, G.C. Zhang, C.S. Zhou, S.L. Gao. *J. Anal. Appl. Pyrol.*, **99**, 66 (2013).
[15] B.D. Wu, J.G. Zhang, T.L. Zhang, L. Yang, Z.N. Zhou. *Eur. J. Inorg. Chem.*, **2012**, 1261 (2012).
[16] Q. Zhang, J.M. Shreeve. *Angew. Chem. Int. Ed. Engl.*, **53**, 2540 (2014).
[17] S. Li, Y. Wang, C. Qi, X. Zhao, J. Zhang, S. Zhang, S. Pang. *Angew. Chem. Int. Ed. Engl.*, **52**, 14031 (2013).
[18] M.A. Ilyushin, N.A. Petrova, I.V. Tselinsky. *Chin. J. Energy Mater.*, **1**, 41 (1993).
[19] I.A. Ugryumov, M.A. Ilyushin, I.V. Tselinskii, A.S. Kozlov. *Russ. J. Appl. Chem.*, **76**, 439 (2003).
[20] M.A. Ilyushin, I.V. Tselinskiy, A.V. Smirnov, I.V. Shugalei. *Cent. Eur. J. Energy Mater.*, **9**, 3 (2012).
[21] J.T. Wu, J.G. Zhang, X. Yin, M. Sun, T.L. Zhang. *Z. Anorg. Allg. Chem.*, **639**, 2354 (2013).
[22] H.E. Kissinger. *Anal. Chem.*, **29**, 1702 (1957).
[23] T. Ozawa. *Bull. Chem. Soc. Jpn.*, **38**, 1881 (1965).
[24] G.M. Sheldrick. *SHELXS-97, Program for the Solution of Crystal Structure*, University of Gottingen, Germany (1990).
[25] G.M. Sheldrick. *Acta Crystallogr., Sect. A: Found. Crystallogr.*, **64**, 112 (2008).
[26] G.M. Sheldrick. *SHELXL-97, Program for the Solution of Crystal Structure*, University of Gottingen, Germany (1997).
[27] M.J. Frisch, G.W. Trucks, H.B. Schlegel. *Gaussian 03 (Revision A.01)*, Gaussian Inc., Pittsburgh, PA (2003).
[28] M.J. Frisch, J.A. Pople, J.S. Binkley. *J. Chem. Phys.*, **80**, 3265 (1984).
[29] B. Yan, H.Y. Li, N.N. Zhao, H.X. Ma, J.R. Song, F.Q. Zhao, R.Z. Hu. *J. Chem. Eng. Data*, **58**, 3033 (2013).
[30] G.B. Rong, S.Z. Zu. *Structure Determination of Organic Compounds Tables of Spectral Data*, East China University of Science and Technology Press, Shanghai (2002).
[31] R.Z. Hu, Z.Q. Yang, Y. Liang. *Thermochim. Acta*, **123**, 135 (1988).
[32] B.D. Wu, Y.G. Bi, Z.N. Zhou, L. Yang, J.G. Zhang, T.L. Zhang. *J. Coord. Chem.*, **66**, 3014 (2013).